**G. Lee-Glauser**
Research Assistant,
Department of Mechanical and Aeronautical Engineering,
Clarkson University,
Potsdam, NY 13699
Assoc. Mem. ASME

**Jer-Nan Juang**
Principal Scientist,
Spacecraft Dynamics Branch,
NASA Langley Research Center,
Hampton, VA 23665
Mem. ASME

**J. L. Sulla**
Senior Engineer,
Lockheed Engineering and Sciences Company,
Hampton, VA 23665

# Optimal Active Vibration Absorber: Design and Experimental Results

*An optimal active vibration absorber can provide guaranteed closed-loop stability and control for large flexible space structures with collocated sensors/actuators. The active vibration absorber is a second-order dynamic system which is designed to suppress any unwanted structural vibration. This can be designed with minimum knowledge of the controlled system. Two methods for optimizing the active vibration absorber parameters are illustrated: minimum resonant amplitude and frequency matched active controllers. The Controls-Structures Interaction Phase-1 Evolutionary Model at the NASA Langley Research Center is used to demonstrate the effectiveness of the active vibration absorber for vibration suppression. Performance is compared numerically and experimentally using acceleration feedback.*

## Introduction

Recently, active vibration absorbers (AVA), or virtual passive controllers, have received much attention for the vibration suppression of large flexible space structures. This is largely due to the AVA controller's ability to guarantee closed-loop stability with minimum knowledge of the controlled system. The theoretical development of the AVA controller and actual implementation are reported by Bruner et al. (1992), Juang and Phan (1992a), Juang et al. (1991), Morris and Juang (1990), and Williams et al. (1992).

In this study, two methodologies of optimal tuning of the AVA controller are studied and compared. The first controller uses the minimization of the resonant amplitude as shown by Juang (1984). The second controller uses the frequency match of the absorber to the controlled system as shown by Bruner et al. (1992). These methods are then used to design the AVA controller for the Controls-Structures Interaction (CSI) Phase-1 Evolutionary Model (CEM Phase-1). The simulation and experimental results of these two methods are compared to see which method gives better vibration suppression without actuator saturation. Both numerical and experimental results will be shown by using sinusoidal and random excitations. Open/closed-loop modal parameters are identified using the Observer/Kalman Filter Identification (OKID) software described by Juang et al. (1993). The open/closed-loop damping ratios are compared.

In the following sections, we start with a short review of the AVA controller developed by Juang and Phan (1992a). The two optimal tuning methods for the AVA controller are shown and discussed in terms of a physical interpretation. Then, a brief description of the real time control is presented. Finally, numerical and experimental results are shown and discussed. A conclusions section closes the paper.

## AVA Controller

The equations of motion for control of large flexible space structures are typically written as

$$M\ddot{x}+D\dot{x}+Kx=Bu \tag{1}$$

$$y=H_a\ddot{x}+H_v\dot{x}+H_dx \tag{2}$$

where $x$ is an $n \times 1$ displacement vector and the mass, stiffness, and damping matrices satisfy $M = M^T > 0$, $K = K^T \geq 0$, and $D = D^T \geq 0$, respectively. In the absence of rigid-body motion, $K = K^T > 0$. Here $B$ is an $n \times p$ influence matrix which describes the actuator force distributions for the $p \times 1$ control vector $u$. Equation (2) represents a $m \times 1$ measurement vector $y$, and $H_a$, $H_v$, and $H_d$ are the $m \times n$ acceleration, velocity, and displacement influence matrices, respectively.

Let the AVA controller take a similar form as Eqs. (1) and (2), then

$$M_c\ddot{x}_c+D_c\dot{x}_c+K_cx_c=B_cu_c \tag{3}$$

and

$$y_c=H_{ac}\ddot{x}_c+H_{vc}\dot{x}_c+H_{dc}x_c. \tag{4}$$

The above equations do not represent any physical system since it is a fictitious model. Here $x_c$ is an $n_c \times 1$ controller displacement vector, and $M_c$, $D_c$, and $K_c$ can be interpreted as the controller mass, damping, and stiffness matrices, respectively. These are symmetric and positive definite in general mechanical systems, so that the controller is asymptotically stable. The $n_c \times m$ influence matrix $B_c$ describes the force

Contributed by the Technical Committee on Vibration and Sound for publication in the JOURNAL OF VIBRATION AND ACOUSTICS. Manuscript received April 1993; revised Sept. 1993. Technical Editor: D. J. Inman.

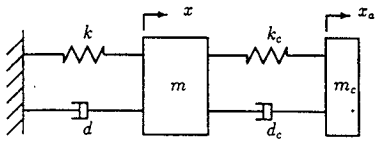


**Fig. 1 A single degree-of-freedom plant model with a single degree-of-freedom controller**

distributions for the $m \times 1$ input force vector $u_c$. Equation (4) represents the $p \times 1$ controller measurement vector $y_c$, and $H_{ac}$, $H_{vc}$, and $H_{dc}$ are the $p \times n_c$ acceleration, velocity, and displacement influence matrices, respectively. The controller design parameters are the quantities $M_c$, $D_c$, $K_c$, $B_c$, $H_{ac}$, $H_{vc}$, and $H_{dc}$. Let the flexible space structure and the controller be interconnected so that the output of the controller is the input to the structure, and the output of the structure is the input to the controller, i.e.,

$$u = y_c = H_{ac}\ddot{x}_c + H_{vc}\dot{x}_c + H_{dc}x_c \tag{5}$$

$$u_c = y = H_a\ddot{x} + H_v\dot{x} + H_d x \tag{6}$$

Upon substitution of Eqs. (5) and (6) into Eqs. (1) and (3), respectively, the overall closed-loop system equation becomes

$$M_t\ddot{x}_t + D_t\dot{x}_t + K_t x_t = 0 \tag{7}$$

where

$$M_t = \begin{bmatrix} M & -BH_{ac} \\ -B_cH_a & M_c \end{bmatrix},$$

$$D_t = \begin{bmatrix} D & -BH_{vc} \\ B_cH_v & D_c \end{bmatrix},$$

$$K_t = \begin{bmatrix} K & -BH_{dc} \\ -B_cH_d & K_c \end{bmatrix}, \qquad x_t = \begin{bmatrix} x \\ x_c \end{bmatrix}$$

The control equation is modified and the actuators/sensors locations are adjusted to design a controller that is model-independent and ensures stability of the closed-loop system regardless of any perturbations. Only the special case of acceleration feedback is considered in this study, i.e., ($H_v$, $H_d \equiv 0$). By proper selection of $H_{ac}$ and $B_c$, the above equation produces a symmetric closed-loop mass matrix, $M_t$. To insure that $M_t$ is positive definite, the input force in Eq. (5) is modified to include a direct acceleration feedback, i.e.,

$$u = y_c - G_a y = H_{ac}\ddot{x}_c - G_aH_a\ddot{x} \tag{8}$$

where, $G_a$ is a gain matrix defined as

$$G_a = H_{ac}M_c^{-1}B_c \tag{9}$$

Let sensors and actuators be collocated in this study such that

$$B = H_a^T \text{ and } H_{ac} = B_c^T \tag{10}$$

and $B_c$ be defined as

$$B_c = M_c\bar{B}_c \text{ or } \bar{B}_c = M_c^{-1}B_c \tag{11}$$

then closed-loop mass matrix becomes

$$M_t = \begin{bmatrix} M + H_a^T\bar{B}_c^TM_c\bar{B}_cH_a & -H_a^T\bar{B}_c^TM_c \\ -M_c\bar{B}_cH_a & M_c \end{bmatrix} \tag{12}$$

which is symmetric and positive definite as long as $M$ and $M_c$ are positive definite.

In this paper, a single degree-of-freedom with an acceleration feedback AVA controller is considered as shown in Fig. 1. Therefore, the controller design is a set of scalar designs which neglects all other actuators and sensors interactions. For the collocated sensors/actuators, let $\bar{B}_c = H_a = 1$. A state space form for the single degree-of-freedom system to be controlled can be written as

$$\dot{\tilde{x}} = A\tilde{x} + By \qquad u = C\tilde{x} + Dy \tag{13}$$

where

$$A = \begin{bmatrix} 0 & 1 \\ -k/m & -d/m \end{bmatrix}, \qquad B = \begin{bmatrix} 0 \\ 1/m \end{bmatrix},$$

$$C = [-k/m \quad d/m], \qquad D = [1/m], \qquad \tilde{x} = \begin{bmatrix} x \\ \dot{x} \end{bmatrix}$$

These parameters are used for an optimal AVA design for performance only. If the structural modal parameters are not known accurately, the AVA closed-loop system design still guarantees stability but not performance as desired. The controller matrices can be written so that the vector $x_c$ represents the relative position between $m_c$ and $m$. The corresponding controller equations in a state form are

$$\dot{\tilde{x}}_c = A_c\tilde{x}_c + B_cy_c \qquad u_c = C_c\tilde{x}_c + D_cy_c \tag{14}$$

where

$$A_c = \begin{bmatrix} 0 & 1 \\ -k_c/m_c & -d_c/m_c \end{bmatrix}, \qquad B_c = \begin{bmatrix} 0 \\ 1 \end{bmatrix},$$

$$C_c = [-k_c \quad -d_c], \qquad D_c = [0], \qquad \tilde{x}_c = \begin{bmatrix} x_c \\ \dot{x}_c \end{bmatrix}$$

In the following sections, two methods for optimizing the AVA controller parameters for optimal performance are discussed.

**Minimum Resonant Amplitude AVA.** The AVA Controller is optimally designed to minimize the vibration amplitude of the structure. This is achieved by minimizing a quadratic cost function which is the integral of the squared structure deflection, i.e.,

$$2J = \int_0^\infty x^TQx\,dt \tag{15}$$

where $Q = Q^T \geq 0$.

The optimal AVA controller parameter in this case are derived by Juang (1984) and presented in dimensionless form as

$$f = 1/(1+\mu_c) \tag{16}$$

$$\zeta_c = \frac{1}{f}\sqrt{\frac{\mu_c}{4(1+\mu_c)^3}} \tag{17}$$

where the mass ratio is defined as $\mu_c = m_c/m$, $f$ is the frequency ratio of the controller to the system natural frequency for initial displacement case, and $\zeta_c$ is the controller damping ratio. The mass ratio is selected to avoid actuator saturation.

**Frequency Matched AVA.** The AVA controller frequency is "matched" to the driving frequency of the actuator for a desired plant damping ratio, $\zeta_{dp}$; hence, the unwanted vibration energy in the system is absorbed. The coefficient terms of the actual and desired closed-loop characteristic equations are matched. This is shown in the Appendix. This procedure leads to a 6th order polynomial for the frequency ratio, $f$, which is written as

$$f^6(-(1+\mu_c)^2) + f^5(4\zeta_{dp}\zeta_p(1+\mu_c)) + f^4((1+\mu_c)(3-4\zeta_{dp}^2) - 4\zeta_p^2) + f^2(4\zeta_{dp}^2 + 4\zeta_p^2 - 3 - \mu_c) + f(-4\zeta_{dp}\zeta_p) + 1 = 0 \tag{18}$$

where $\zeta_p$ is the actual plant damping ratio. The frequency ratio, $f$, is then used to calculate the desired controller damping ratio, $\zeta_{dc}$, as

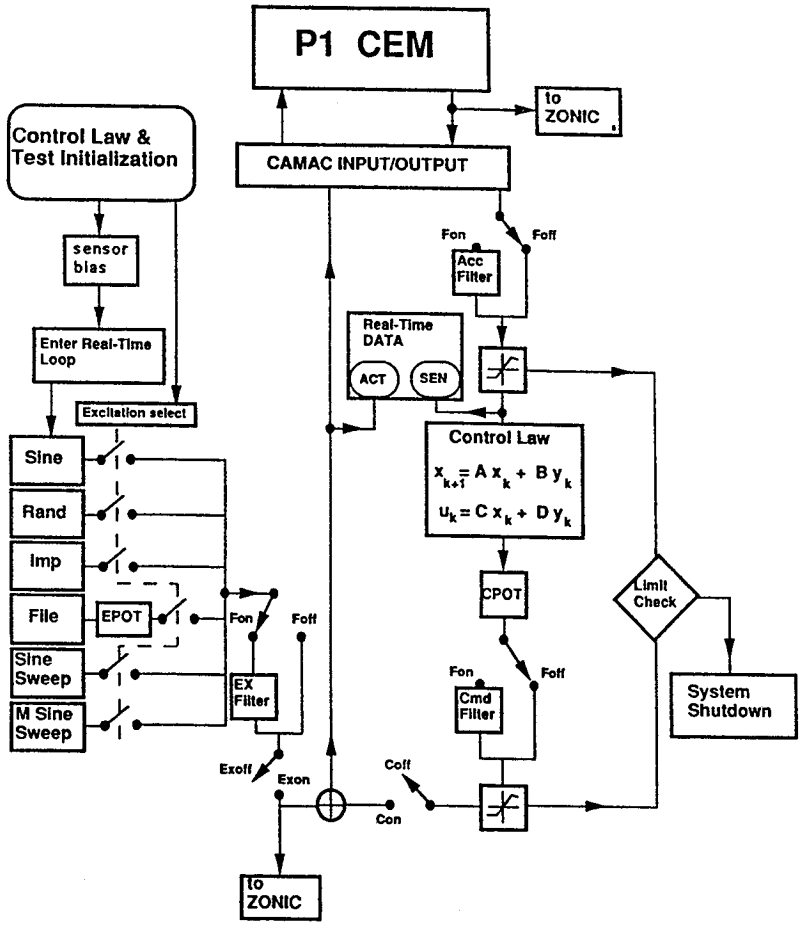


Fig. 2 Flow chart of the real time control logic

$$\zeta_{dc} = \frac{(1+\mu_c - 4\zeta_p^2)f^4 + 4\zeta_p\zeta_{dp}f^3 - 2f^2 + 1}{4\zeta_{dp}f^2 - 4\zeta_p f^3} \tag{19}$$

The optimal $\zeta_{dc}$ is defined as when the difference between $\zeta_{dp}$ and $\zeta_{dc}$ is less than 5 percent. The optimal $\zeta_{dc}$ is achieved by varying $\mu_c$. The actual optimal controller parameters can now be defined through the optimal desired closed-loop parameters as

$$\zeta_c = (\zeta_{dp} + \zeta_{dc})f - \zeta_p f^2 \tag{20}$$

and

$$\omega_c = \omega_p f^2 \tag{21}$$

Here, $\omega_c$ and $\zeta_c$ are the optimal controller natural frequency and damping ratio, respectively. The desired plant damping ratio, $\zeta_{dp}$, is selected to avoid actuator saturation as well as to optimize the controller damping.

## Real Time Control Logic

The flow chart of the real time control logic is shown in Fig. 2. Here, P1 CEM represents the CEM Phase-1. The CAMAC (Computer Automated Measurement and Control) system is used to interface the analog-to-digital and digital-to-analog conversion. More detailed description about CAMAC is shown by Belvin et al. (1991). The rest of the diagram represents the computer software except for the Zonic (ZETA software reference) which is a commercially available data acquisition and signal processing system. The experiment begins by reading the control matrices and test initialization which represents the Control Law & Test Initialization in Fig. 2. The initialization sets the test parameters including test time, sample rate, excitation and control times, excitation options, controller size, scale factors, and options of digital filtering for actuator commands and sensor outputs. Excitation options are sinusoids, random signals, pulses, user defined excitation, and two sine sweep options. The sine sweep option requires the specifications of start and stop times, sampling frequency, and the number of cycles for each frequency step. On the other hand, the M sine sweep option only requires the specifications of start and stop times, and sweep time. Three digital filters are available for excitation commands (EX Filter), control commands (Cmd Filter), and sensor outputs (Acc Filter) for the user to select and provide with a filter data file. Upon completion of a test initialization, the sensor biases for calibration are calculated by averaging the sensor over 1000 samples, and then the actual real time test begins by using the data file parameters. Thruster commands and sensor outputs are checked per sample for the limit to ensure the controller stability and system safety. When the test is finished, the actuator commands and sensor data are stored as a MATLAB binary file.

## Numerical and Experimental Results

The aforementioned AVA Controller design methods are used to control the first ten modes of the CEM Phase-1. Figure 3 shows a schematic of the model and the location of 8 collocated sensors/actuators. The finite element model and experimental mode shapes are used as a guide to determine the sensor/actuator pair location to control specific modes. The actuators at locations 1, 2, 4, and 8 are used to control two independent modes. For this case, two independent optimal AVA controllers are designed, but in the application, the first target mode is the primary mode to be controlled.

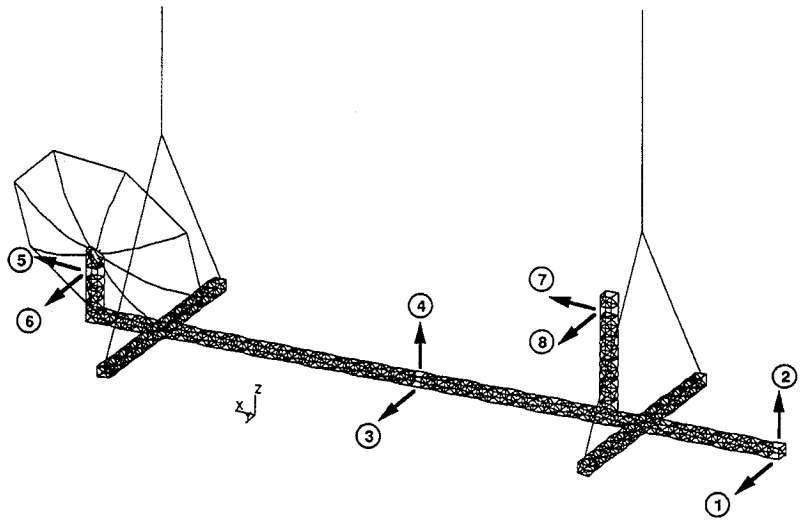


Fig. 3 Schematic of the CEM Phase-1 showing collocated sensor and actuator locations

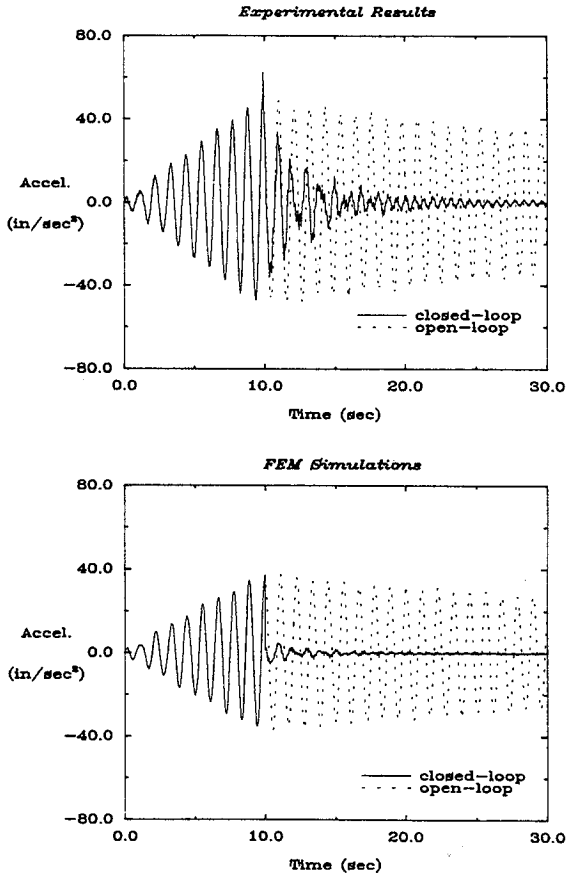


Fig. 4 Open/closed-loop experimental results and FEM simulations of the minimum resonant amplitude AVA controller at sensor 8 for the system excited by actuator 8 with sinusoidal input of the frequency at mode 6

**(A) AVA Controller Design.** The AVA controller designs are demonstrated by first exciting the CEM Phase-1. A sinusoidal excitation is used to excite individual modes of the model to estimate individual modal parameters for the AVA designs with optimal performance. This is then used to design both a minimum resonant amplitude and a frequency matched AVA controllers. Both controller parameters are selected to avoid actuator saturation. The AVA controller design parameters under the above conditions are shown in Tables 1 and 2. For the open-loop case, the structure is excited by using a sinusoidal excitation at the individual frequencies of interest for the duration of each test. For the closed-loop case, the structure is excited with open-loop conditions for the first 10 or 15 seconds then the AVA controller is activated. Mode 6 is used as an example. Figures 4 and 5 show the results of the minimum resonant amplitude and the frequency matched AVA controllers for mode 6, respectively. The dotted and solid lines represent the open and closed-loop conditions, respectively. Both FEM simulation and the experimental results show a similar trend of time histories for mode 6 in these figures. The effectiveness of both AVA controllers are clearly demonstrated in these figures. The frequency matched AVA controller is somewhat faster in suppressing vibration than the minimum resonant amplitude AVA controller. For clarity, closed-loop impulse response simulations are used to compare the AVA controllers which is shown in Fig. 6. These results also indicate that the frequency matched AVA controller is somewhat more effective in vibration suppression.

Table 1 Minimum resonant amplitude AVA controller design parameters

| Sensor/Actuator location | 1st Target Mode | | | 2nd Target Mode | | |
|---|---|---|---|---|---|---|
| | $m_c$ | $d_c$ | $k_c$ | $m_c$ | $d_c$ | $k_c$ |
| 1 | 2.000 | 0.743 | 0.524 | 0.055 | 0.120 | 13.687 |
| 2 | 0.300 | 0.470 | 4.164 | 0.200 | 0.290 | 3.253 |
| 3 | 0.057 | 0.123 | 14.201 | – | – | – |
| 4 | 0.670 | 1.005 | 9.830 | 0.450 | 0.612 | 7.670 |
| 5 | 2.200 | 0.804 | 1.300 | – | – | – |
| 6 | 0.320 | 0.462 | 28.579 | – | – | – |
| 7 | 1.500 | 0.545 | 0.898 | – | – | – |
| 8 | 0.100 | 0.157 | 2.708 | 0.045 | 0.075 | 3.949 |

Table 2 Frequency matched AVA controller design parameters

| Sensor/Actuator location | 1st Target Mode | | | 2nd Target Mode | | |
|---|---|---|---|---|---|---|
| | $m_c$ | $d_c$ | $k_c$ | $m_c$ | $d_c$ | $k_c$ |
| 1 | 2.000 | 1.473 | 0.472 | 0.100 | 0.591 | 24.074 |
| 2 | 0.310 | 0.991 | 4.220 | 0.330 | 1.103 | 4.530 |
| 3 | 0.110 | 0.659 | 26.428 | – | – | – |
| 4 | 0.700 | 2.144 | 10.086 | 0.700 | 2.191 | 10.576 |
| 5 | 2.400 | 1.840 | 1.311 | – | – | – |
| 6 | 0.600 | 2.346 | 51.368 | – | – | – |
| 7 | 1.700 | 1.307 | 0.925 | – | – | – |
| 8 | 0.150 | 0.544 | 3.705 | 0.090 | 0.411 | 7.406 |

**(B) Effectiveness of AVA Controller.** The effectiveness

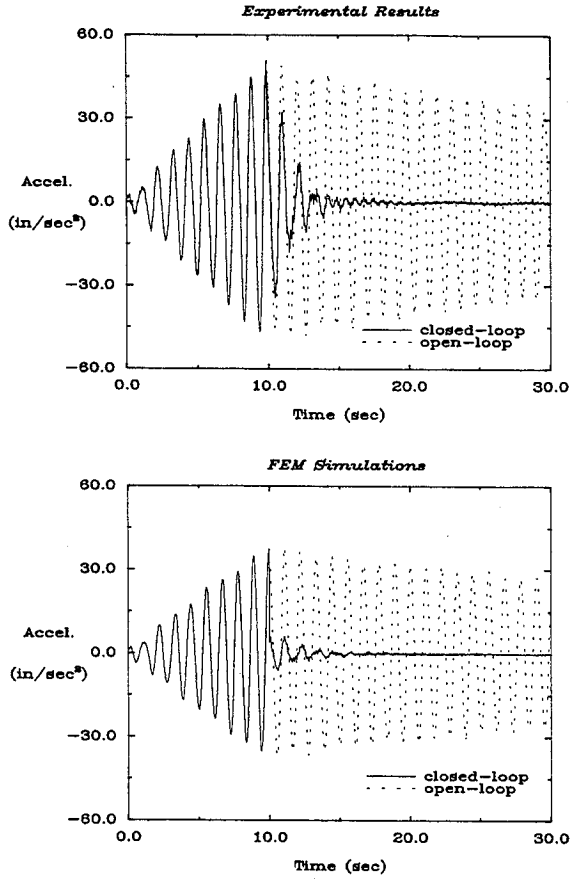


**Fig. 5 Open/closed-loop experimental results and FEM simulations of the frequency matched AVA controller at sensor 8 for the system excited by actuator 8 with sinusoidal input of the frequency at mode 6**

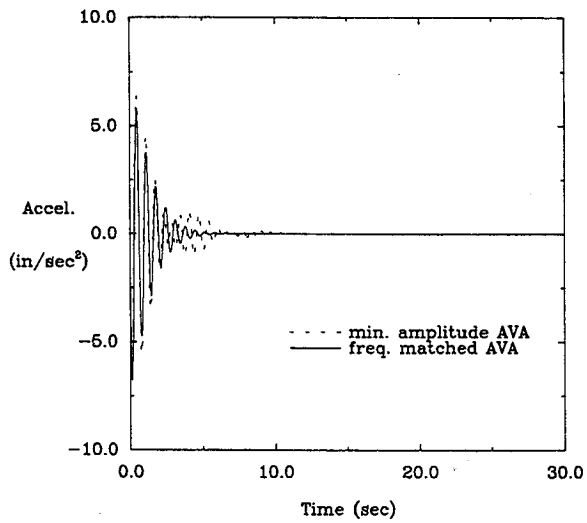


**Fig. 6 Open/closed-loop impulse response simulations at sensor 8 for the system excited by actuator 8 with sinusoidal input of the frequency at mode 7**

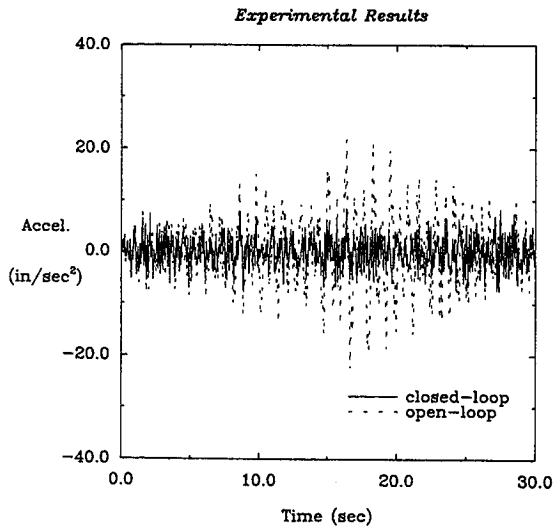


**Fig. 7 Open/closed-loop experimental results of the frequency matched AVA controller at sensor 8 under random input at all 8 actuators**

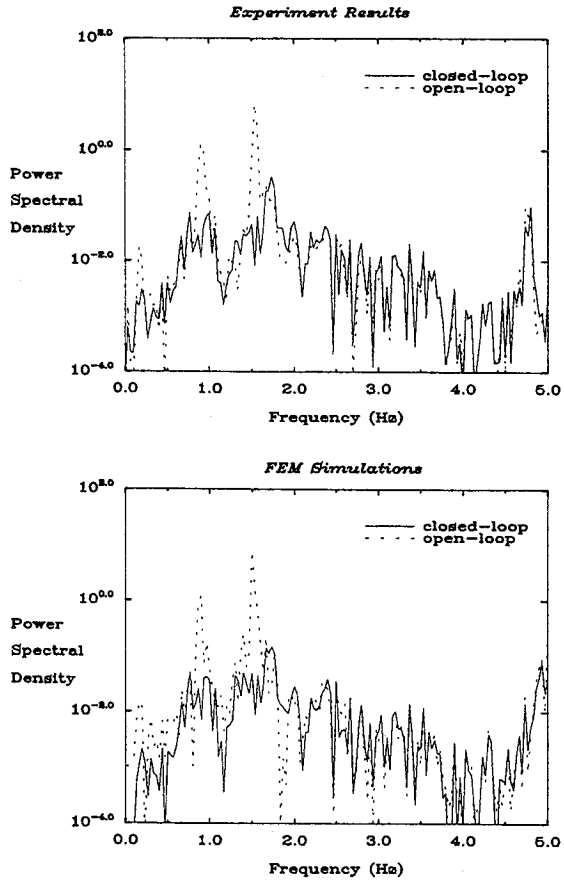


**Fig. 8 Open/closed-loop power spectral densities of the experimental results and FEM simulations for the minimum resonant amplitude AVA controller at sensor 8 under random excitation at all 8 actuators**

of the minimum resonant amplitude and frequency matched AVA controllers are also demonstrated under random excitations, which controls 24 states with 8 inputs and 8 outputs with a 200 Hz sampling rate. The white, zero-mean and Gaussian random signal, with 5 Hz cut-off frequency, is used to excite the structure. Sensor 8, shown in Fig. 7, is used as a typical example of the open/closed-loop experimental results under random input. The peak response of the AVA controllers is approximately 50 percent less than the open-loop response for both experimental results and FEM simulations. The power spectral densities (PSD) plots of the signals from Sensor 8 are shown in Fig. 8 for the minimum resonant amplitude AVA controller. Figure 9 shows the PSD plots for the frequency matched AVA controller. These PSD show the vibration energy reduction of the controlled modes. The purpose of these plots, which are not Bode plots, is to better illustrate the difference in the amplitude of the spectral densities between the open and

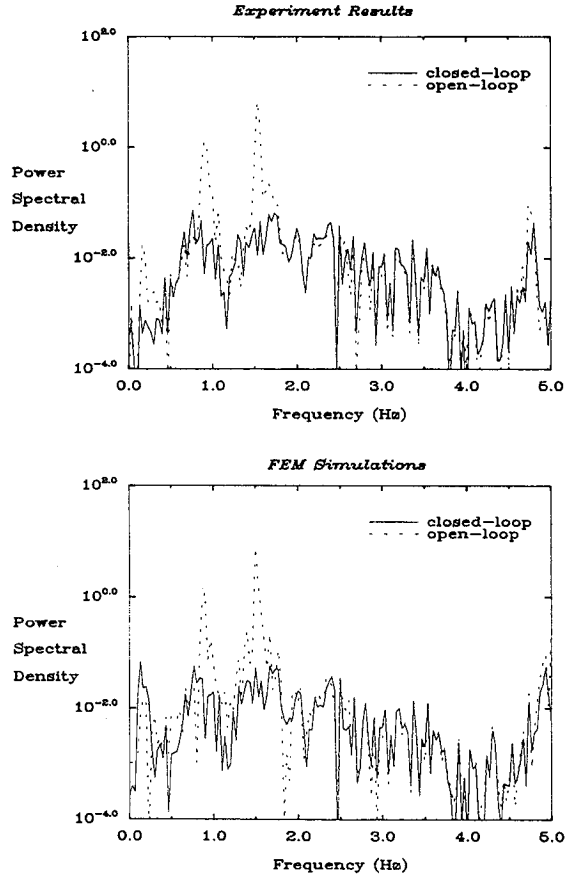


**Fig. 9 Open/closed-loop power spectral densities of the experimental results and FEM simulations for the frequency matched AVA controller at sensor 8 under random excitation at all 8 actuators**

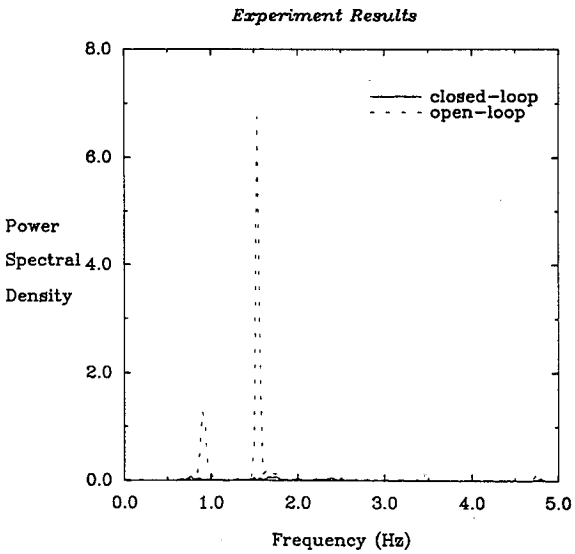


**Fig. 10 Open/closed-loop power spectral densities of the experimental results for the frequency matched AVA controller at sensor 8 under random excitation at all 8 actuators**

closed-loop systems. The power spectral density of the frequency matched AVA controller for sensor 8, plotted on a linear scale, is shown in Fig. 10 to demonstrate the effectiveness of the AVA controller in reducing the vibrations of modes 6 and 7 with frequencies of .911 Hz and 1.54 Hz, respectively. Figure 10 definitely shows that modes 6 and 7 are suppressed by the AVA controller. In general, the FEM simulation results

**Table 3 Comparison of open/closed loop damping**

| Frequency (Hz) | Damping (%) | | | | |
|---|---|---|---|---|---|
| | Sinusoidal Excitation | | Random Excitation | | |
| | Open-loop | Closed-loop | OKID Open-loop | OKID Closed-loop Min. Amp. | OKID Closed-loop Freq. Matched |
| .158 | 3.8 | 32.0 | - | - | - |
| .172 | 7.0 | 60.0 | - | - | - |
| .720 | .90 | 22.0 | 1.15 | 31.12 | 58.18 |
| .737 | .97 | 24.0 | 1.69 | 27.29 | 21.98 |
| .911 | .42 | 20.0 | .64 | 5.58 | 10.75 |
| 1.54 | .45 | 11.0 | 1.04 | 10.01 | 12.08 |
| 2.56 | .50 | 10.0 | 1.03 | 9.29 | 11.0 |

are in good agreement with the experimental results for both controllers. These figures also indicate that the frequency matched AVA controller is somewhat more effective in vibration suppression than the minimum resonant amplitude AVA controller.

**C. System Identification using OKID.** Open/closed-loop modal parameters from experimental data are identified using the OKID. Table 3 shows the comparison of the open/closed-loop damping ratios for the sinusoidal and random excitations. The closed-loop damping ratios for the sinusoidal excitation represent the specified damping ratio for both AVA controllers. Even under the random excitation, the OKID closed-loop damping ratios are in reasonable agreement with the specified damping ratios. The OKID did not have a long enough experimental record to identify the lower frequencies. This table also shows that the damping ratios increased significantly from the open-loop to the closed-loop system, which is a primary factor for the vibration suppression.

## Conclusions

Two methods, the minimum resonant amplitude and the frequency matched, for tuning the active vibration absorber (AVA) parameters are demonstrated and evaluated. The effectiveness of these AVA controllers are tested using the Controls Structures Interaction Phase-1 Evolutionary Model. Experimental and simulation results show both AVA controllers being very effective in suppressing the vibrations. The frequency matched AVA controller suppresses the vibration somewhat faster than the minimum resonant amplitude AVA controller. The frequency matched AVA controller produces more realistic actuator commands without actuator saturation. The experimental results demonstrate the robustness of the AVA controller designs by being able to control 24 states under random excitations.

## Acknowledgment

This work is supported by NASA Langley Aerospace Research Summer Scholars (LARSS) program through Hampton University Grant NCC 1-106.

## References

1 Belvin, W. K, Elliott, K., Horta, L., Bailey, J., Bruner, A., Sulla, J., Won, J., and Ugoletti, R., 1991, "sl Langley's CSI Evolutionary Model: Phase 0," *NASA TM-104165*, Langley Research Center, Nov.

2 Bruner, A. M., Belvin, W. K., Horta, L. G., and Juang, J.-N., 1992, "Active Vibration Absorber for the CSI Evolutionary Model: Design and Experimental Results," *Journal of Guidance, Control, and Dynamics*, Vol. 15, No. 5, Sept.-Oct., pp. 1253-1257.

3 Juang, J.-N., and Phan, M., 1992a, "Robust Controller Designs for Second-Order Dynamic Systems: A Virtual Passive Approach," *Journal of Guidance, Control, and Dynamics*, Vol. 15, No. 5, Sept.-Oct., pp. 1192-1198.

4 Juang, J.-N., Wu, S.-C., Phan, M., and Longman, R. W., 1991, "Passive Dynamic Controllers for Non-Linear Mechanical Systems," *NASA TM-104047*, Langley Research Center, March, *Journal of Guidance, Control, and Dynamics, in press.*

5 Juang, J.-N., 1984, "Optimal Design of a Passive Vibration Absorber for a Truss Beam," *Journal of Guidance, Control, and Dynamics*, Vol. 7, No. 6, Nov.-Dec.

6 Juang, J.-N., Phan, M., Horta, L. G., and Longman, R. W., 1993, "Identification of Observer/Karman Filter/Markov Parameters: Theory and Experiments," *Journal of Guidance, Control, and Dynamics*, Vol. 16, No. 2, March–April, pp. 320–329.

7 Morris, K. A., and Juang, J.-N., 1990, "Dissipative Controller Designs for Second-Order Dynamic Systems," *NASA Contractor Report 187452*, September, *IEEE Transaction in Automatic Control, in press*.

8 Williams, T. W. C., Xu, J., and Juang, J.-N., 1992, "Design of Virtual Passive Controllers for Flexible Structures," *Proc. of AIAA/AAS Astro Dynamics Conf.*, Hilton Head, South Carolina, Aug. 10–12, pp. 217–226.

9 Zonic A & D Engineering and Test Analysis (ZETA) Software Reference, Park 50 TechneCenter, 25 Whitney Drive, Milford, OH 45150.

## APPENDIX

Derivation of the frequency matched AVA controller parameters are shown in this Appendix. The equation of motion for the system shown in Fig. 1 is

$$m\ddot{x}+d\dot{x}+kx-d_c\dot{x}_c-k_cx_c=0 \tag{A.1}$$

$$m_c\ddot{x}_c+d_c\dot{x}_c+k_cx_c+m_c\ddot{x}=0 \tag{A.2}$$

where $x_c = x_a - x$. The closed-loop characteristic equation of this system becomes

$$s^4+s^3\left(\frac{d_c}{m}+\frac{d_c}{m_c}+\frac{d}{m}\right)+s^2\left(\frac{dd_c}{m_cm}+\frac{k_c}{m_c}+\frac{k_c}{m}+\frac{k}{m}\right)+s\left(\frac{k_cd}{m_cm}+\frac{kd_c}{m_cm}\right)+\frac{kk_c}{m_cm}=0 \tag{A.3}$$

The frequency matched desired plant and controller characteristic equation is written as

$$(s^2+2\zeta_{dp}\omega s+\omega^2)(s^2+2\zeta_{dc}\omega s+\omega^2)=0 \tag{A.4}$$

and its expanded form is

$$s^4+s^3(2\zeta_{dc}\omega+2\zeta_{dp}\omega)+s^2(2\omega^2+4\zeta_{dp}\zeta_{dc}\omega^2)+s(2\zeta_{dp}\omega^3+2\zeta_{dc}\omega^3)+\omega^4=0 \tag{A.5}$$

Now, the coefficient terms are matched to define the controller parameters. The $s^0$ term is

$$\frac{k_c}{m_c}=\frac{\omega^4}{\omega_p^2} \tag{A.6}$$

where $\omega_p^2 = k/m$. The $s^1$ term is

$$\frac{d_c}{m_c}=\frac{2}{\omega_p^2}\left(\zeta_{dp}\omega^3+\zeta_{dc}\omega^3-\zeta_p\frac{\omega^4}{\omega_p}\right) \tag{A.7}$$

where $d/m = 2\zeta_p\omega_p$. The $s^2$ term is

$$\zeta_{dc}=\frac{(1+\mu_c-4\zeta_p^2)f^4+4\zeta_p\zeta_{dp}f^3-2f^2+1}{4\zeta_{dp}f^2-4\zeta_pf^3} \tag{A.8}$$

where $\mu_c = m_c/m$ and $f = \omega/\omega_p$. The $s^3$ term is

$$f^6(-(1+\mu_c)^2)+f^5(4\zeta_{dp}\zeta_p(1+\mu_c))+f^4((1+\mu_c)(3-4\zeta_{dp}^2)-4\zeta_p^2)+f^2(4\zeta_{dp}^2+4\zeta_p^2-3-\mu_c)+f(-4\zeta_{dp}\zeta_p)+1=0 \tag{A.9}$$